International Journal of Mass Spectrometry 288 (2009) 6–15

Contents lists available at ScienceDirect

International Journal of Mass Spectrometry

journal homepage: www.elsevier.com/locate/ijms

Exploring rearrangements along the fragmentation pathways of diuron anion: A combined experimental and computational investigation

Basem Kanawati*, Mourad Harir, Philippe Schmitt-Kopplin

Institute of Ecological Chemistry, Helmholtz Center Munich, German Research Center for Environmental Health, Ingolstädter Landstr.1, D-85758 Neuherberg, Germany

ARTICLE INFO

Article history:
Received 2 December 2008
Received in revised form 15 July 2009
Accepted 17 July 2009
Available online 7 August 2009

Keywords:
DCMU
DFT
FT-ICR
Energy barrier
Fragmentation mechanism

ABSTRACT

Diuron (3-(3,4-dichlorophenyl)-1,1-dimethylurea), a common herbicide from phenyl urea class, was investigated by studying the formation of several negative ions $[M-H]^-$ in the gas phase and the fragmentation behaviour of the thermodynamically most probably formed isomeric anions upon linear ion acceleration/collision experiments. The collision induced dissociation experiments (CID) were carried out in a hexapole–quadrupole–hexapole hybrid system coupled to 12 T magnet with infinity ICR cell for high resolution measurements. Two distinctive main pathways were observed in the MS/MS spectrum. Sustained off-resonance irradiation (SORI) experiments inside the ICR cell reinforce the fragmentation channels obtained from linear ion acceleration experiments. The fragmentation pathways were also completely investigated by the use of B3LYP/6-311+G(2d,p)//B3LYP/6-31+G(d) level of theory. Elimination of dimethylamine takes place in a two-step process, by which two successive 1,3 proton shifts occur. The second 1,3 proton shift is concerted with the departure of dimethylamine. The driving force for the $(CH_3)_2NH$ elimination is the formation of isocyanate group. The formed primary product ion can further decompose to release HCl through a new transition state. A stable new aromatic product ion is formed with 10π electrons. Loss of C_3H_5NO neutral from another anionic isomer of the precursor ion was also observed and is characteristic for the amide terminal of the diamide functional group. A concerted mechanism is proposed, by which N–C bond breakage and cyclization of the eliminated neutral fragment C_3H_5NO takes place simultaneously to form 1-methyl-aziridin-2-one.

1. Introduction

Diuron (3-(3,4-dichlorophenyl)-1,1-dimethylurea), known also as DCMU is a substituted urea-based herbicide, which represents an important class of contact herbicides widely used for weeds' control [1]. Due to its moderate water solubility of 22–42 mg/L at 20 °C, DCMU leaks slowly to the terrestrial layers causing groundwater [2], reservoir water and rivers [3] contamination. Its potential risk is the inhibitory effect of hill reaction in photosynthesis by limiting the production of high-energy compounds which can be used for various metabolic processes [4–6].

Biodegradation of DCMU was intensively investigated in soil by actinomycetes [7], fungi [8] and by UV light [9]. Different analytical methods were implemented for these studies, but no computational (theoretical) studies of gas phase ion fragmentation of DCMU ions were performed to gain structural elucidation of the compound from a mass spectrometric point of view.

The density functional theory (DFT) has witnessed an intensive development and its applications in various chemical problems become of great interest. B3LYP functional with the basis set 6-31+G(d) for geometry optimizations was used, due to the well accuracy of 6-31+G(d) level of theory (when combined with 6-311+G(2d,p) basis set for single point energy calculations) and the computationally moderate time consumption [10]. It was also implemented to elucidate intramolecular rearrangements in complex sesquiterpene oxidation products which bear multiple organic functional groups [11] as well as for inorganic applications [12,13]. Chandra and Uchimaru [14] used B3LYP to calculate the C–H bond dissociation enthalpies of several haloalkanes. They found that the B3LYP functional has an average error of 1.2 kcal/mol when combined with the basis set 6-311G(d,p). Furthermore, B3LYP/6-31+G(d,p) was found to give very reliable results for predicting the acidities of nucleobases [15].

The B3LYP functional [16,17] with the basis set 6-31+G(d) was not only implemented to study closed shell ions in the literature but also to study radical ions. Grützmacher et al. used the basis set 6-31+G(d) for geometry optimizations to investigate ion–molecule reactions between halogenated radical cations and alcohols in a combined DFT/FT-ICR-MS study [18]. In another DFT/FT-ICR study, the same level of theory could give an accurate insight about

* Corresponding author. Tel.: +49 89 3187 2412.
E-mail address: Basem.Kanawati@helmholtz-muenchen.de (B. Kanawati).
URLs: http://www.kanawati.de (B. Kanawati), http://www.helmholtz-muenchen.de/ioec/.

1387-3806/$ – see front matter © 2009 Elsevier B.V. All rights reserved.
doi:10.1016/j.ijms.2009.07.010

ion–molecule reactions between 2-bromopropene radical cation and amines in the gas phase [19]. Naumov et al. studied transformations of 5-membered heterocyclic radical cations by low temperature electron paramagnetic resonance EPR spectroscopy. In their recent study, they utilized DFT UBHLYP/6-31+G(d) level of theory to calculate hyperfine splitting (hfs) constants and found a very good agreement between the measured and calculated values of the hfs constants [20]. Mariano et al. investigated several halogenated species with negative electron affinities by DFT methods and concluded that B3LYP/6-311+G(2df,p)//B3LYP/6-31+G(d) gave a good correlation between the experimental data and theoretical values [21].

DCMU as well as other herbicides were previously investigated in the positive electrospray ionization mode coupled to HPLC and different mass spectrometric analyzers [22,23]. Unlike the gas phase chemistry of positive ions, very little is known in regard to negative ionic species, especially in concern to their reactivity and fragmentation behaviour. DePuy et al. described some chemical reactions of anions in flowing afterglow apparatus [24]. They also described ion–molecule reactions of organic anions and their corresponding neutrals [25]. A fundamental review about fragmentation of several classes of negative organic ions exists [26]. Negative chemical ionization of organic molecules is also given as a review in the literature [27].

Kanawati et al. showed in previous studies [28,29], that the difference in single point energy results obtained from 6-311++G(3df, 3pd) and 6-311+G(2d,p) is minimal (lower than 1.5 kcal/mol) for closed shell ionic systems, when the energy differences are averaged along a complete reaction path. Calculations with both basis sets give the same trend in the behaviour of energy curves for multi-steps fragmentation pathways.

Deuterium experiments are not always helpful in deciphering gas phase reaction mechanisms, especially in cases, where collisionally activated ion dissociations take place. This is due to the fact, that energy supply on the parent ion can induce rapid D/H scrambling processes [30–32] before the fragmentation can take place. Jorgensen et al. [33] have shown in a Q-TOF-MS that complete intramolecular randomization of all hydrogen atoms attached to nitrogen and oxygen in the amide functional groups with deuterium occurs in the gaseous peptide ion prior to its dissociation under low collisional energy activation conditions. Thus, the quantum mechanical approach is necessary for understanding the fragmentation mechanisms.

The aim of this study is not only to show detailed mechanistic pathways, which are in agreement with experimental mass spectrometric results, but also to reveal new synthetic pathways for logical recombination of negative organic ions and neutrals, which can be of interest to retro synthetic organic chemists. The ion structures and their pathways of formation were studied by using two complementary approaches: (a) the collision-induced dissociation (CID) experiments and (b) the hybrid DFT method at the B3LYP/6-311+G(2d,p)//B3LYP/6-31+G(d) level of theory. The results obtained from both sources are reported herein and clear fragmentation mechanisms are established.

2. Experimental

An FT-ICR mass spectrometer (Bruker Daltonics, Bremen, Germany) with 12 T magnet (Magnex, UK) was used for the experimental study. Scheme 1 shows the FTMS instrument, which consists of a hexapole–quadrupole–hexapole ion guide, coupled to an infinity ICR cell [34]. In the first hexapole, ions can be accumulated for variable time before they are forwarded to the quadrupole, which serves as a mass filter. Once isolated, the interesting ion can be accelerated in the second hexapole and let to collide with Argon

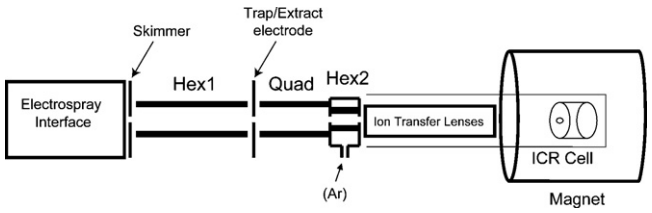

Scheme 1. Schematic representation of the main devices in the FTMS instrument. Hex and Q stand for hexapole and quadrupole respectively.

atoms in the second hexapole, where a relatively high pressure of Argon gas (10^{-2} mbar) is maintained.

The formed product ions together with the remaining precursor ions are subsequently accelerated toward the ICR cell through a series of ion accelerating and decelerating lenses to overcome the magnetic fringing field. Once trapped inside the ICR cell, a dipolar radial excitation pulse can be triggered from the excitation plates of the ICR cell to excite ions radially. This causes an increase in the cyclotron motion of all ions for detection. A time domain transient is obtained with a size of 1 M words and is Fourier transformed to obtain a frequency spectrum, which is then converted by Apex Control program (Bruker Daltonics, Bremen, Germany) to a mass spectrum. All ion excitations were performed in broad band mode (frequency sweep radial ion excitation). Simulations of ion trajectories inside ICR cells in both thermal motion and also during radial excitation are well known and given in the literature [35–37].

Ions were accumulated in the first hexapole for 1 s and in the second hexapole (collision cell) for 100 ms prior to ICR ion detection. The base pressure in the ICR vacuum chamber was 5×10^{-10} mbar and in the quadrupole region 3×10^{-6} mbar. High pressure in the quadrupole region is necessary to co-linearize the ions in the radial plane and decelerate the radial components of the ion kinetic energy.

Sustained off-resonance irradiation experiments were also performed on specific product ions formed as a result of linear ion acceleration and collisional CID experiments (described above). These SORI experiments were performed to reinforce the MS/MS data obtained from the hexapole fragmentation. The deviation from the on-resonance excitation is 500 Hz in the SORI experiment with an excitation pulse duration of 200 ms and amplitude of 2Vp-p. A pulse valve was used for the SORI experiment to provide Argon atoms for the SORI experiment with an open duration of 200 ms.

Electrospray ionization source (Apollo II, Bruker Daltonics, Bremen, Germany) was used in the negative ionization mode to ionize the studied analyte in pure Methanol (Lichrosolv, Sigma–Aldrich, Schnelldorf, Germany). 10 ppm DCMU in Methanol was injected directly to the ionization source by the use of a microliter pump at a flow rate of 2 μL/min. A source heater temperature of 200° was maintained and no nozzle–skimmer fragmentation was performed in the ionization source. The instrument was previously calibrated by the use of Arginine negative cluster ions starting from a methanolic arginine solution of 10 ppm.

3. Calculations

The electronic structure calculations were performed on a stand-alone computer using Density Functional Theory, incorporated in Gaussian 03W program [38]. The hybrid DFT method B3LYP was implemented with the polarization functions 2d for each heavy atom and 1p for each hydrogen atom in all single point energy calculations. All geometry optimizations were performed using 6-31+G(d) basis set. Frequency calculations were also done for each optimized geometry using the same basis set 6-31+G(d) to obtain the zero point vibrational energy (ZPVE). This value is multiplied

by the scaling factor 0.9804 to correct for vibrational anharmonicities [10]. Single point energy (SPE) calculations were done using 6-311+G(2d,p) level of theory. The use of diffuse functions was important to represent the correct geometry of anionic species. Stability tests on all calculated structures were performed to ensure that the used wave function does represent the lowest energy solution of the self consistent field (SCF) equations.

For geometry optimization, a modified conjugate gradient algorithm from Gaussian Inc (Ct, USA) [39] was used in combination with the GDIIS algorithm [40–42]. The requested convergence in the density matrix was 10^{-8}, the threshold value for maximum displacement was 0.0018 Å, and that for the maximum force was 0.00045 Hartree/Bohr. The nature of the stationary points was established by calculating and diagonalizing the Hessian matrix (force constant matrix). Transition structures were characterized through normal-mode analysis (frequency analysis). The transition vector associated with the unique imaginary frequency has been determined in each found transition state and is provided as animation in Appendix B supplementary material. This vector represents the eigenvector associated with the unique negative eigenvalue of the force constant matrix, which indicates that the found structure corresponds to a first order saddle point (transition state). In order to further check that the found transition state really connects two energy minima structures with each other (reactant with product), intrinsic reaction coordinate [43] (IRC) calculations in all found transition state geometries, were performed in mass-weighted internal coordinates [44].

For Nucleas Independent Chemical Shift (NICS) calculations [45], the standard NMR GIAO method [46,47] was used with HF/6-31+G(d) level of theory on the 6-31+G(d) optimized geometries. All geometries of electronic structures calculated were rendered by GaussView program [48]. Mechanistic studies for isodesmic transformations (gas phase intramolecular rearrangements and ion fragmentation processes) are presented in this paper.

4. Results and discussion

Fig. 1A shows the MS/MS fragmentation pattern of the produced $[M-H]^-$ ion m/z 231 of DCMU at collision energy of 15 eV in the laboratory frame. Only the monoisotopic signals are labelled in Fig. 1A. Ion m/z 231 indicates the sum formula $C_9H_9N_2OCl_2$. This ion can fragment in two different pathways. In the first pathway it can fragment to produce the product ion m/z 186 with the sum formula $C_7H_2Cl_2NO$. The measured mass difference is 45.05783 and indicates the sum formula C_2H_7N with an absolute error of 0.05 milli mass unit (mmu), indicating that the departing neutral is dimethylamine $(CH_3)_2NH$. Once formed, the primary product ion $[M-H-(CH_3)_2NH]^-$ m/z 186 can further fragment losing HCl to give rise to a secondary product ion with a nominal m/z of 150. The measured mass difference 35.97668 indicates the sum formula HCl with an absolute error of only 0.05 mmu. These two mass differences are too accurate so that their absolute errors are much less than the mass of one electron m/z 0.55 mmu. This shows the great advantage of ICR high resolution measurements for obtaining very narrow signals which give highly accurate masses.

Fig. 1B shows the result of a SORI experiment performed on the primary product ion m/z = 186 $[M-H-Me_2NH]^-$ anion, which is produced by linear CID of $[M-H]^-$ ion m/z 231 in the hexapole. As Fig. 1B shows, no product ion m/z = 160 is formed from ion m/z = 186. This indicates that ion m/z = 160 is a primary product ion which is formed from ion m/z = 231 directly due to linear CID in the hexapole.

Fig. 2 shows experimental and calculated isotopic patterns of the formed product ions. A perfect match between the measured and the calculated isotopic patterns is achieved. The second fragmentation pathway is also shown in Fig. 1B and indicates the loss of a neutral with a mass of 71.03721 which corresponds to the sum formula C_3H_5NO with an absolute mass error of 0.12 mmu. The isotopic pattern for the product ion m/z 160 affirms also the sum formula $C_6H_4Cl_2N$ for this product ion. Based on the accurate sum formulas, ion m/z 160 ($C_6H_4Cl_2N$) cannot be formed starting from the primary fragment ion m/z 186 ($C_7H_2Cl_2NO$), since ion m/z 186 contains only two hydrogen atoms, whereas ion m/z 160 contains 4 hydrogen atoms. The SORI experiment shown in Fig. 1B reinforces this fact. DFT calculations discussed below show a completely logical mechanistic pathway for the elimination of the C_3H_5NO from $[M-H]^-$ $C_9H_9N_2OCl_2$ m/z 231 to give a primary product ion m/z 160 with the sum formula $C_6H_4Cl_2N$.

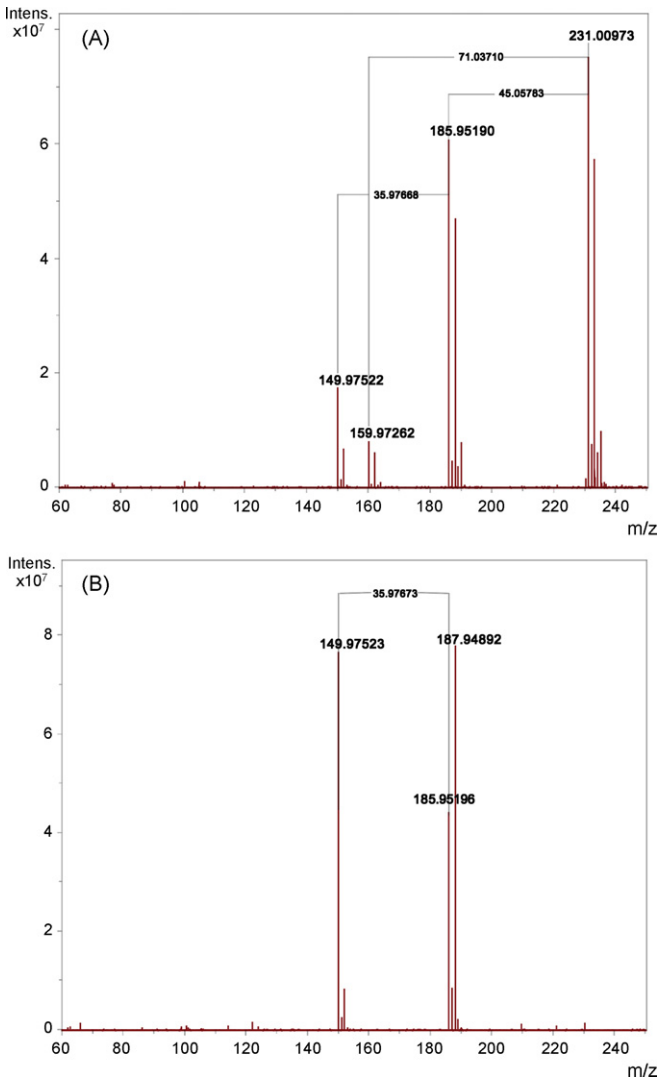

Fig. 1. (A) MS/MS fragmentation pattern of $[M-H]^-$ m/z 231 of DCMU at collision energy of 15 eV (laboratory frame) in the hexapole. (B) SORI MS/MS spectrum of isolated $[M-H-Me_2NH]^-$ anion m/z = 186. This ion was obtained by linear CID applied on $[M-H]^-$ m/z = 231 in the collision cell (hexapole).

4.1. Isomeric anions for $[M-H]^-$ m/z 231 of DCMU

Fig. 3 shows the optimized geometries of five anionic isomers of $[M-H]^-$ of DCMU. These isomer anions are the result of theoretical deprotonation from several sites of neutral molecule of DCMU. Table 1 gives gas phase site dependent deprotonation energies. As shown in Table 1, it is clear that proton removal from the internal nitrogen of the alkylated urea is thermodynamically the

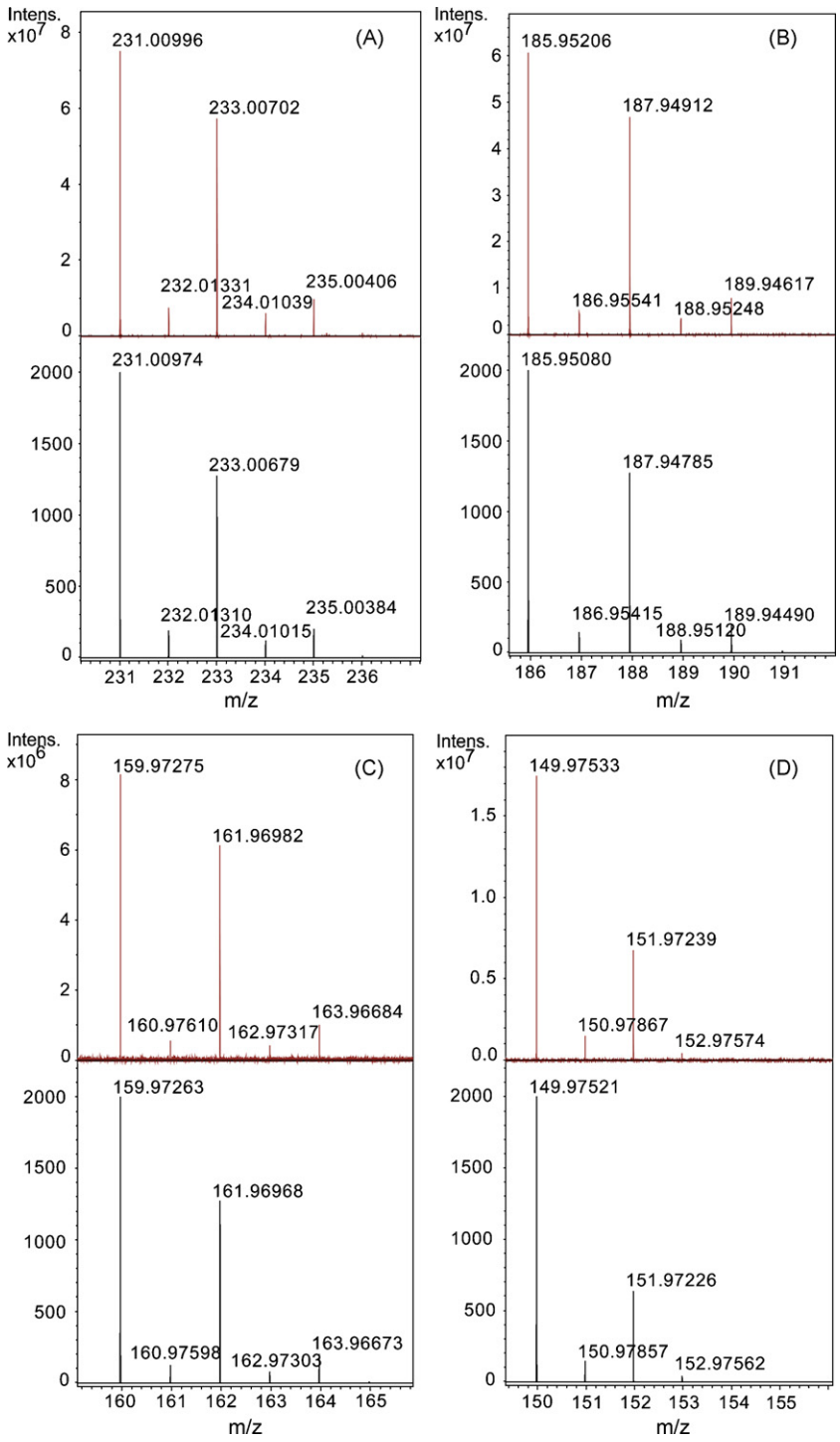

Fig. 2. Measured and simulated isotopic patterns for (A) the precursor ion *m*/*z* 231 and all formed product ions (B–D) as a result of collision induced dissociation experiment performed at 15 eV in the collision cell (hexapole).

most favourable event for ionization in the Electrospray source. The hydrogen atoms in the benzene ring are not acidic enough to initiate deprotonation. This is obvious from the energies required to form Anions 1–3 with deprotonation energies of 368, 380 and 374 kcal/mol, respectively. Although proton removal from one of the two methyl groups connected to the external amidic nitrogen atom has high-energy demand, Anion 5 cannot be excluded, since it is possible to be formed as a result of two body collision between Anion 4 and the DCMU neutral. This ion–molecule reaction is endothermic (as expected) by 52.4 kcal/mol and can be driven by ion acceleration between the electrospray needle and the counter electrode (skimmer) in the ionization source. We will show in the next sections that both isomers (Anion 4 and Anion 5) play an important role in drawing two distinctive main fragmentation pathways, which delineate the structure of DCMU.

5. DFT mechanistic study for $(CH_3)_2NH$ and HCl eliminations

After we showed that the most probable isomer formed for $[M-H]^-$ ion *m*/*z* 231 of DCMU in the ion source is Anion 4, the elimination of dimethylamine from Anion 4 is not possible, since

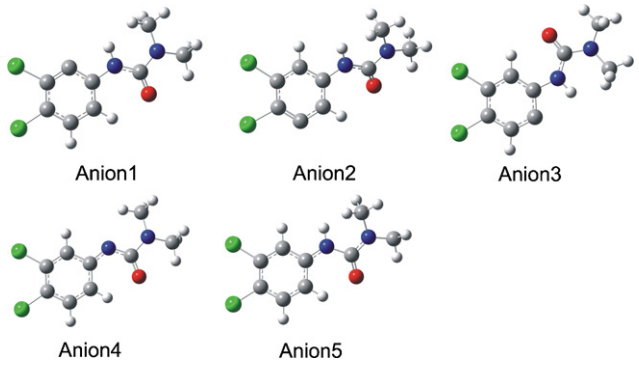

Fig. 3. Optimized geometries of several isomeric anions for $[M-H]^-$ m/z 231 of DCMU.

Table 1
Gas phase deprotonation energies of $[M-H]^-$ isomeric anions of DCMU.

Isomer	E (Hartree)	DP B3LYP/6-311+G(2d,p)
Anion 1	−1453.559075	368
Anion 2	−1453.539995	380
Anion 3	−1453.549508	374
Anion 4	−1453.610789	335
Anion 5	−1453.527205	388

the external amide terminal lacks an additional hydrogen atom that is necessary to connect to the departing $(CH_3)_2N$ moiety to produce dimethylamine. However, there is no hydrogen atom in proximity to the external amide group in Anion 4. Thus, a suitable way for dimethylamine elimination starting from Anion 4 is a two-step process, by which isomerisation from Anion 4 to Anion 1 takes place in the first step through gas phase intramolecular 1,3 proton shift. This is accompanied with a forward energy barrier height of 51.2 kcal/mol and is possible, since Anion 4 is accelerated and let to collide with Argon atoms in the collision chamber. Under a relatively high pressure condition in the collision cell (10^{-2} mbar in the hexapole) more than one collision is highly probable, so that multi internal energy depositions can occur.

The estimated average of internal energy deposited in Anion 4 is $51.2/345.6 \times 100 = 14.8\%$, since Anion 4 is accelerated with 15 eV, which is equivalent to 345.6 kcal/mol electric field supplied kinetic energy. For 15 eV acceleration in the laboratory frame, the center of mass energy (E_{cm}) is equal to $E_{cm} = E_{lab} \times M_t/(M_t + M_p) = 15 \times 40/(40 + 231) = 2.2$ eV = 50.7 kcal/mol, when Argon atoms are used as a collision gas. M_t is the mass of one neutral of the collision gas (target) and M_p is the mass of the accelerated ion (projectile). The center of mass energy $E_{cm} = 2.2$ eV is the maximum amount of deposited internal energy in one collision. Given that the calculated forward energy barrier height (TS1, Fig. 4) is 51.2 kcal/mol = 2.2 eV, we conclude that the first 1,3 proton shift shown in Fig. 4 is feasible. More collisions can deposit more internal energy into the accelerated ion or quench further accelerations depending on the gas pressure. We showed in previous linear ion acceleration studies that the percentage of conversion from kinetic to internal energy can even reach 26% [11,28] relative to the laboratory frame gained energy in quadrupole devices. Thus, internal energy deposition is possible and the energy is invested in inducing

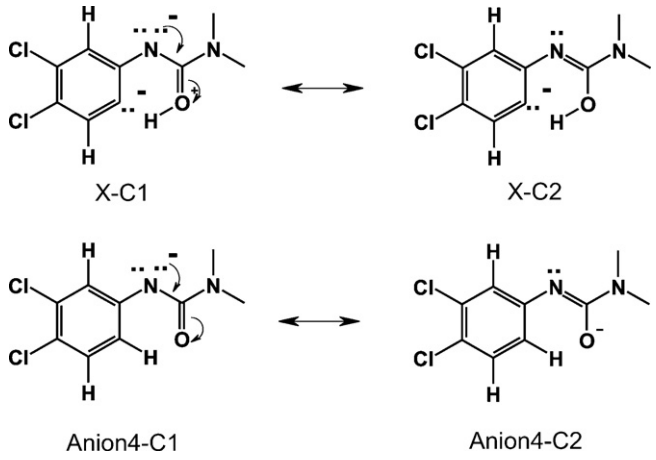

Scheme 2. Canonical forms for Anion 4 and the hypothetical Anion *X*.

gas phase rearrangement prior to fragmentation. Once formed, Anion 1 has a hydrogen atom in proximity to $(CH_3)_2N$ moiety, which is eliminated in a further step. A successive deposition of internal energy by further collisions of the accelerated ions with Argon gas can induce $(CH_3)_2NH$ elimination in a concerted mechanism with an additional 1,3 proton shift (forward energy barrier TS2 = 77.9 − 32.5 = 45.4 kcal/mol, Fig. 4). The driving force for the dimethylamine elimination is the stabilization of the formed primary product ion $[M-H-(CH_3)_2NH]^-$ m/z 186 by electron delocalization in the isocyanate moiety [49].

The primary product ion with isocyanate group can be subsequently further accelerated to eliminate HCl. This requires overcoming an energy barrier height of 83.3 − 44.1 = 39.2 kcal/mol to form an ion-neutral complex with very low reverse energy barrier (83.3 − 81.1 = 2.2 kcal/mol). The detachment of the hydrogen atom and the separation of HCl require 30.6 kcal/mol of energy. The formed secondary product ion $[M-H-(CH_3)_2NH-HCl]^-$ m/z 150 has 10π electrons in a cyclic conjugated system and therefore aromatic. Diefenbach and Schwarz predicted also a high electron density C_6H_6 tetra anion ring with 10π electrons, stabilized as a complex by two Barium ions [50]. In their previous work, they suggested that such a tetra-ion may be produced by an electron source that can supply four additional electrons to the benzene ring. In our findings, we report the formation of a (10π electrons) aromatic mono-charged ionic ring by electrospray deprotonation followed by HCl elimination, which was observed in the MS/MS fragmentation pattern of $[M-H]^-$ of DCMU.

Another alternative mechanism for dimethylamine elimination from Anion 4 would be a 1,5 proton shift of an ortho-proton from the benzene ring to the carbonyl oxygen atom of the alkylated urea moiety as shown in Eq. (1). However, this McLafferty-like 1,5-proton shift through a pseudo 6-membered ring is not possible, since it leads to sharp charge separations which is thermodynamically unfavourable.

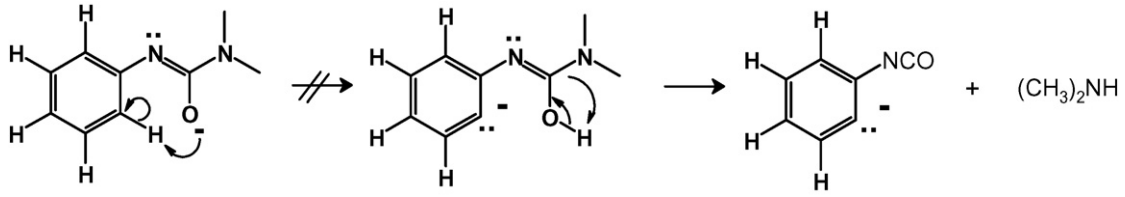

(1)

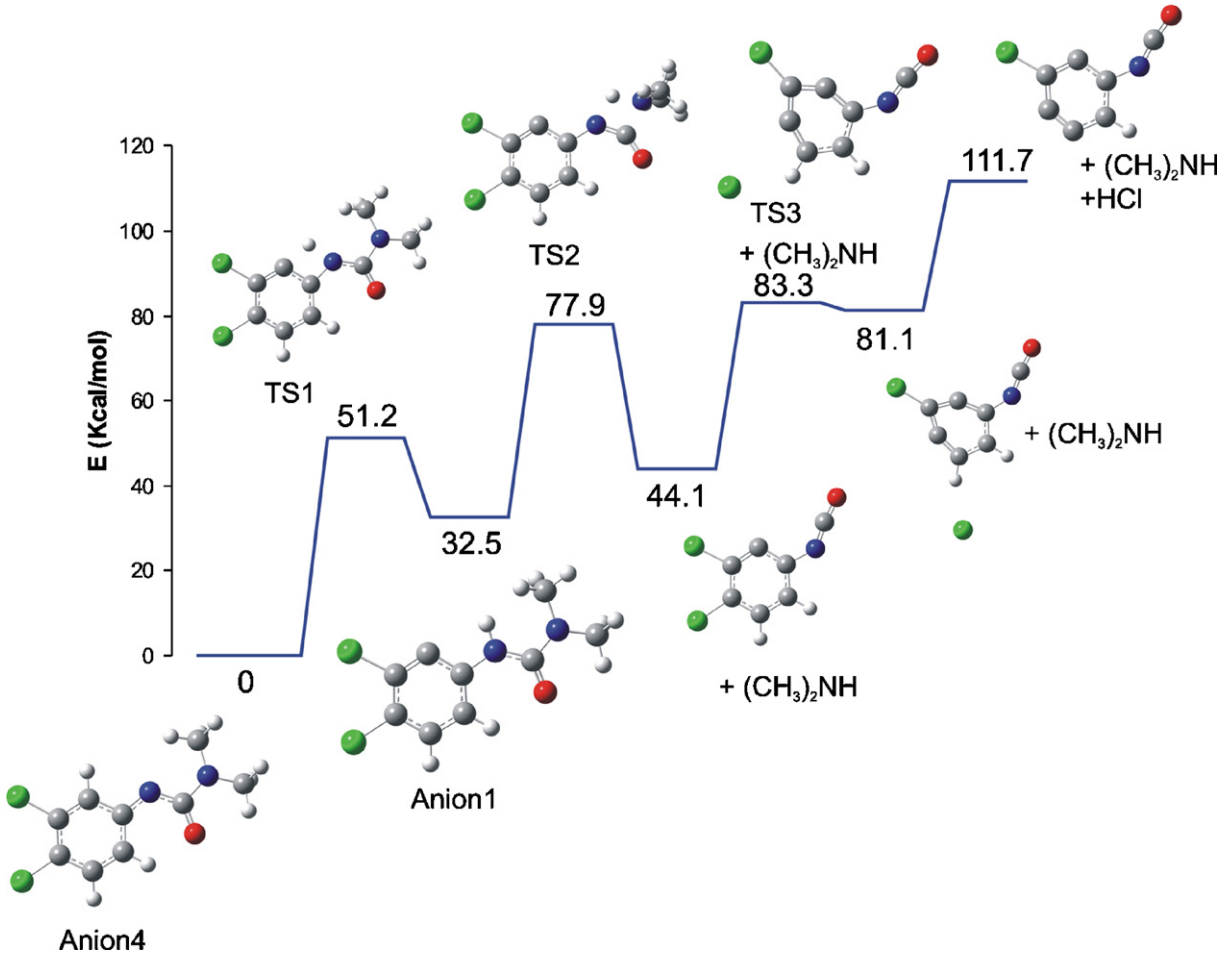

Fig. 4. Energy profile for dimethylamine elimination starting from Anion 4 $[M-H]^-$ m/z 231 and optimized geometries of intermediates and transition states along this pathway, which finally leads to HCl loss.

Scheme 2 shows that one of the canonical forms of the ion formed after this 1,5 proton shift (X-C1) has three charges in three different positions (unstable canonical form), whereas Anion 4 has only stable canonical forms. Quantum mechanical calculations based on both DFT-B3LYP and MP2 methods failed not only to find a transition state for this rearrangement but also failed to stabilize the ion formed after this 1,5 proton shift as energy minimum. It was not possible to optimize the geometry of the formed ion as energy minimum neither with 6-31+G(d,p) nor with higher basis sets [6-311+G(d,p)]. Fig. 5 shows a potential energy curve for the forbidden 1,5 proton shift. The energy difference between the two ionic forms (H bound to C versus H bound to the carbonyl's oxygen atom) is 62.8 kcal/mol. This energy difference is higher than the highest net energy barrier height indicated in Fig. 4 for pathway 1 (51.2 kcal/mol). Thus, Anion *X* whereby the proton is bound to the carbonyl's oxygen atom cannot be formed and is even not stable as an energy minimum structure. The scan coordinate in the shown energy curve is the angle C3–N9–H23 from 48° to 77°. Angle C3–N9–H23 = 50 represents Anion 4, whereas angle C3–N9–H23 = 75° represent the instable Anion *X*.

6. Elimination of C_3H_5NO from $[M-H]^-$ ion

The loss of C_3H_5NO cannot be initiated from any isomeric anion 1,2,3,4 of $[M-H]^-$ m/z 231, since all these four isomer anions contain six hydrogen atoms in the terminal $N(Me)_2$ moiety.

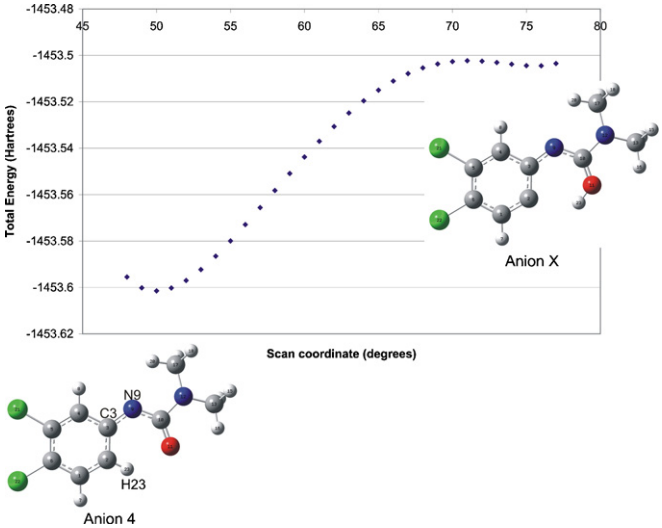

Fig. 5. Potential energy curve for the forbidden 1,5 proton shift discussed in Eq. (1).

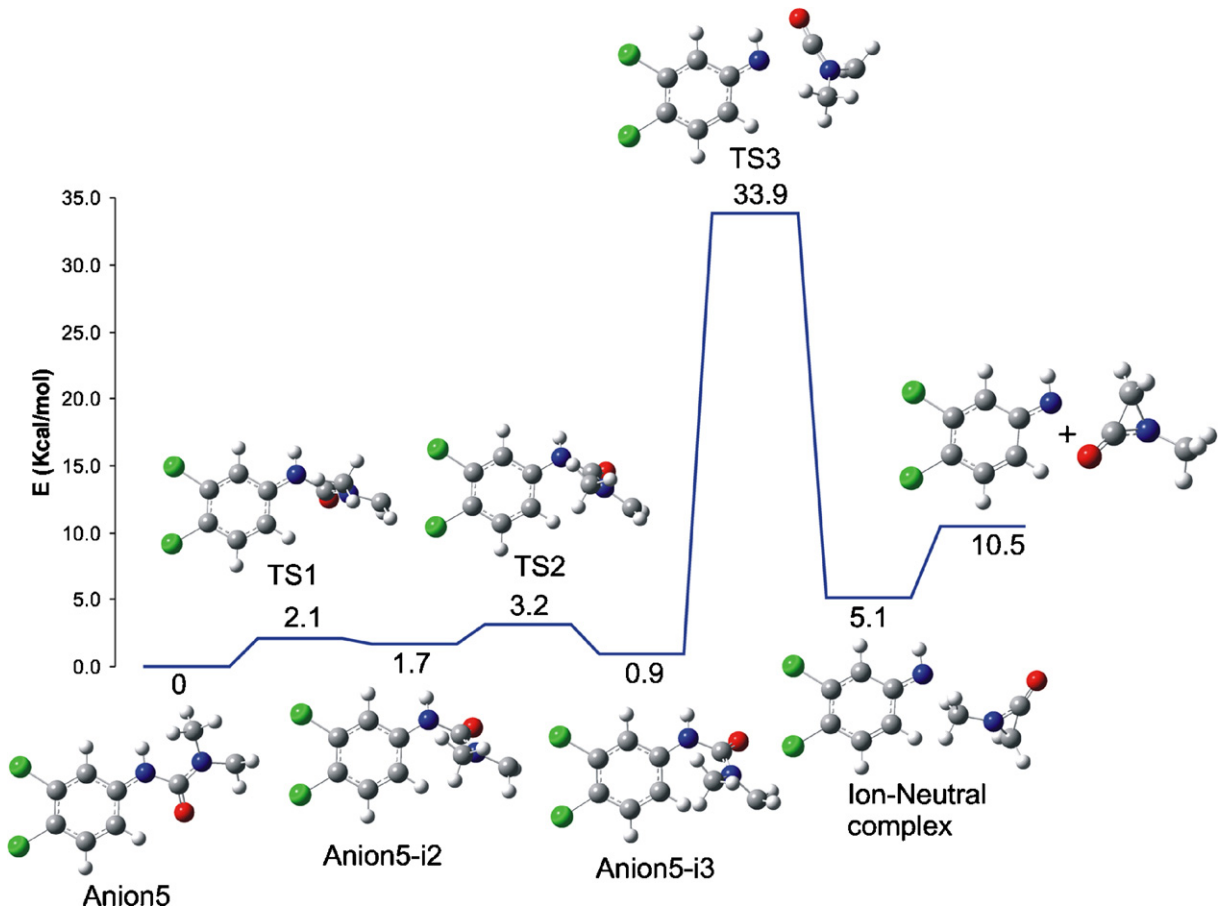

Fig. 6. Energy profile for conformational change and isomerism of Anion 5 $[M-H]^-$ m/z 231 prior to elimination of C_3H_5NO to form the primary product ion m/z 160.

Any attempt to eliminate C_3H_5NO neutral from Anion 4 by 1,4 proton shift fails (Eqs. (2) and (3)).

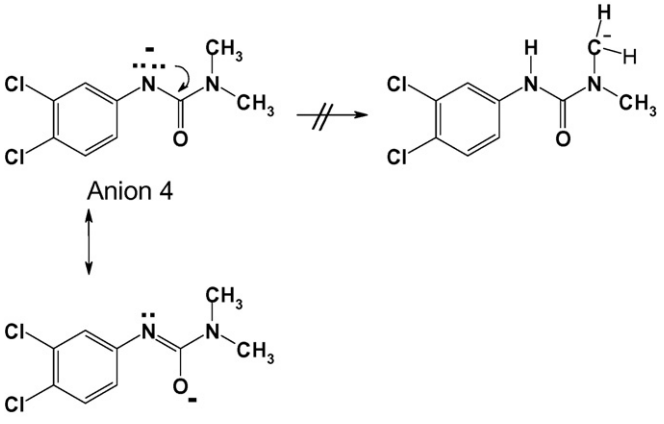

(2)

Eq. (3) cannot proceed, since it is too endothermic. The endothermicity of this reaction is 47.9 kcal/mol. This high endothermicity is due to the production of three separated particles starting from one single precursor ion. This required energy is significant when compared to the more feasible pathway discussed later and shown in Fig. 6 (10.5 kcal/mol endothermic).

The high endothermicity of Eq. (3) prevents this fragmentation, since it is even higher than the energy barrier shown in Fig. 6 for the more feasible pathway through TS3 (see below).

The external methyl group, which has the syn orientation relative to the internal amidic nitrogen atom, cannot be deprotonated by the internal nitrogen atom, which bears the negative charge in Anion 4 (as indicated in Eq. (2)). Neither a transition state for Eq. (2) could be found nor the deprotonated methyl structure is stable as an energy minimum structure. This is a forbidden 1,4 proton shift, since the negative charge would in this case be transferred to the terminal methylene group which is not stable. Note that Anion 4 in Eq. (2) is stable due to electron delocalization between the two hetero atoms in the internal amidic group. The hypothetical product in Eq. (2) cannot be stabilized by electron delocalization. Thus, Eq. (2) is not feasible and no C_3H_5NO neutral can be derived from it.

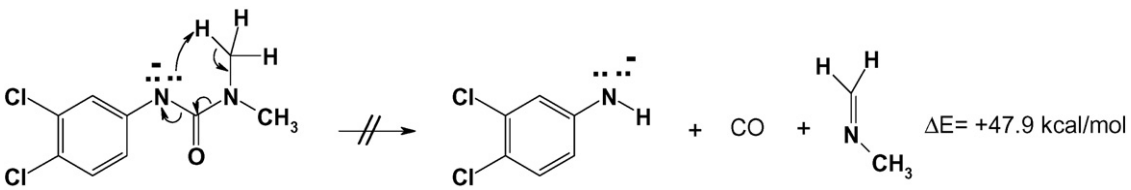

(3)

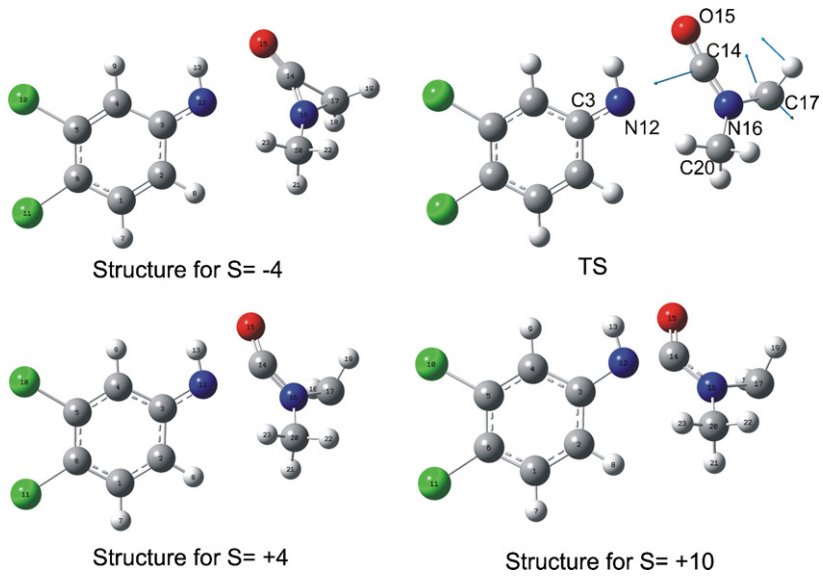

Fig. 7. Structures along the IRC curve shown in Fig. 8 with reaction coordinate values of $S = -4$, +4, 0 and +10. Arrows indicate the transition vectors in the transition state which is responsible of C_3H_5NO elimination/recombination.

Loss of C_3H_5NO is proposed to occur starting from the isomer Anion 5 after two steps of successive conformational changes. These conformational changes are necessary as proved by IRC calculations, which were performed on the found transition states TS1 and TS2 (Fig. 6). The first conformational change indicates a rotation around the N–C bond (between the internal nitrogen and the carbonyl's carbon atom) indicated as TS1, while the second conformational change comprises an inversion of the CH_2 terminal anionic moiety along its C3v symmetry through TS2. Both described changes have negligible forward energy barrier heights of 2.1 kcal/mol for TS1 and 1.5 kcal/mol for TS2. Once the correct conformer is obtained, Anion 5-i3 can then eliminate C_3H_5NO through TS3 in a concerted mechanism with forward energy barrier of 33.9 − 0.9 = 33.0 kcal/mol to give an ion-neutral complex. The released translational energy is high, since the reverse energy barrier for TS3 is significant (33.9 − 5.1 = 28.8 kcal/mol) and is more than sufficient to induce decomposition of the ion-neutral complex to form the product amide ion $Ar{-}NH^-$ (with two electron lone pairs on the terminal nitrogen atom) after C_3H_5NO elimination. The amide anion can be seen as a deprotonated 3,4-dichloroaniline, since this ion $m/z = 160$ give the same fragmentation pattern as $[M{-}H]^-$ anion $m/z = 160$ of 3,4-dichloroaniline. The fragmentation is only represented by HCl elimination to give the product ion $m/z = 124$.

For better illustrating the concerted mechanism, by which C_3H_5NO is eliminated, Fig. 7 shows the structure of TS3 and the structures along the IRC of TS3 at reaction coordinate values of $S = -4$ and $S = +10$. The corresponding IRC energy curve of TS3 is shown in Fig. 8 and provides information about the energy variation along the intrinsic reaction coordinate, which is associated with C_3H_5NO elimination from isomer 5-i3 $[M{-}H]^-$ m/z 231. Plotted energy values are pure electronic energy points (without ZPVE and thermal contributions) calculated on 6-31+G(d) level of theory. Structures on both ends of the coordinate (Fig. 7) do not represent totally optimized energy minima structures. However, these structures illustrate the concerted mechanism for C_3H_5NO elimination through the transition state.

Fig. 8 describes a nucleophilic addition of an aromatic amide ion $Ar{-}NH^-$ on the C=O double bond of the 3-membered heterocyclic ring of 1-methyl-aziridin-2-one, by which a concerted ring opening takes place. According to Hammond principle [51], the asymmetric IRC curve shown in Fig. 8 indicates a product-like transition state, which more resembles the structure for $S = +4$ shown in Fig. 7 previously, since geometries with positive S values have higher energies than those with negative S values. Even when S is extended to reach +10, the potential on the product side of the recombination is higher than the reactant side with $S = -4$. As can be seen from Table 2, the C14–N16–C17 angle remains wide with value of 102.7° in the transition state structure and this resembles the geometry for $S = +4$ more than that for $S = -4$ structure for the same reaction. Note the inversion in the angle C16–C14–C15 along the transition from positive and to negative S values. Unlike Fig. 8, Fig. 6 shows that C_3H_5NO elimination is 5.1 kcal/mol endothermic, while Fig. 8 indicates exothermicity for the same process. However, Fig. 8 does not contradict with Fig. 6, because the structure for $S = -4$ (Fig. 7) is not the optimal optimized geometry. The true stationary point in the negative direction of the intrinsic reaction coordinate is actually the ion-neutral complex shown in Fig. 6, which is slightly higher in energy than 5-i3 anion. This is an example which shows that ion-neutral complex formation can alter what is seen on normal IRC potential curves. Note the structural geometrical differences

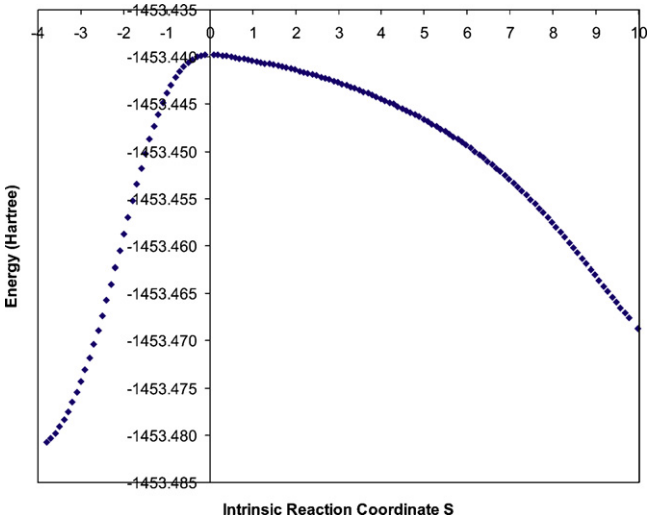

Fig. 8. Absolute potential energy values along the IRC of TS3, which describes the recombination of $C_6H_4NCl_2$ anion with C_3H_5NO in a concerted mechanism.

Table 2
Variation of active geometry parameters along the IRC curve shown in Fig. 7. Bond lengths are in picometer and bond angles are in degrees. The transition from $S = +10$ to $S = -4$ indicates C_3H_5NO elimination. The reverse transition is recombination.

S	N12–C14	C14–C17	C3–N12	C14–N16–C17	C16–C14–C15
−4	325.9	156.1	132.8	68.6	211.3
−3	319.0	167.9	132.9	75.4	205.9
−2	308.5	184.4	133.2	85.1	195.5
−1	298.7	199.7	133.4	94.4	185.6
0	288.7	213.8	133.8	102.7	174.2
1	270.8	229.0	134.4	111.7	160.5
2	258.0	232.7	134.8	113.9	155.3
3	246.0	235.5	135.2	115.5	151.2
4	234.4	237.9	135.8	116.8	147.5
5	222.9	240.3	136.4	118.0	144.1
6	211.2	242.8	137.2	119.2	140.7
7	199.1	245.4	138.2	120.4	137.2
8	186.7	248.2	139.4	121.7	133.6
9	174.5	250.6	140.5	122.8	130.1
10	164.0	251.8	141.1	123.4	127.5

between the ion-neutral complex given in Fig. 6 and the structure for $S = -4$ shown in Fig. 7.

As can be concluded from Fig. 9 and Table 2, the concerted mechanism for C_3H_5NO elimination can be obviously discerned by noticing concomitant N12–C14 bond length increase, C14–C17 bond length decrease as well as decrease in the C14-N16-C17 angle, which indicates the tendency for cyclization of the eliminated moiety at $S = -4$. Table 2 shows also a noticeable shortening of the amidic C3–N12 bond along the elimination pathway. This indicates stabilization of the formed aromatic amide product ion by electron delocalization of one of the nitrogen lone electron pairs with the π electrons of the aromatic benzene ring in 3,4-dichlorophenylamide anion (Scheme 3).

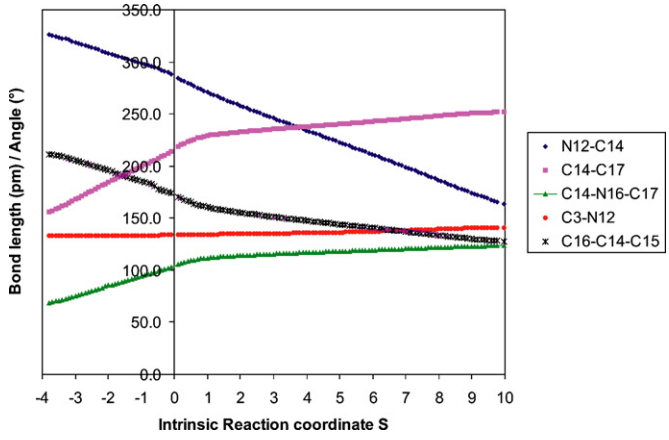

Fig. 9. Variation of specific bond lengths and bond angles along the IRC curve shown in Fig. 8. Bond lengths are given in picometer and bond angles are given in degrees.

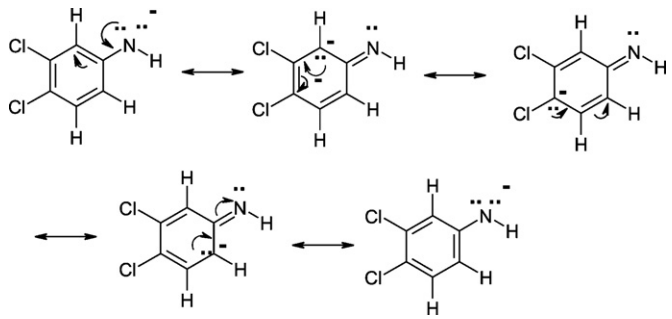

Scheme 3. Canonical forms, which illustrate electron delocalization in the formed primary product anion $C_6H_4NCl_2$.

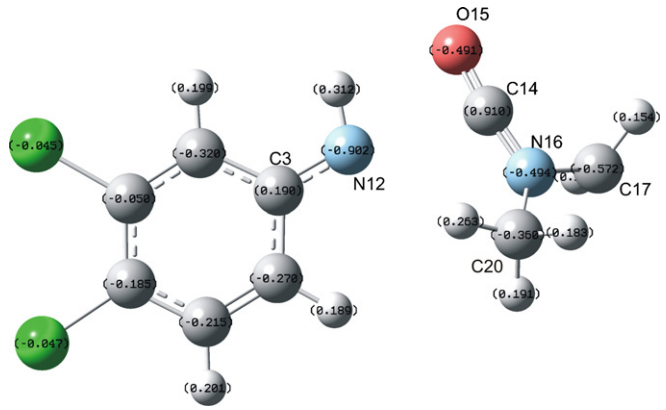

Fig. 10. NBO charge distribution in the transition state, which describes the C_3H_5NO elimination.

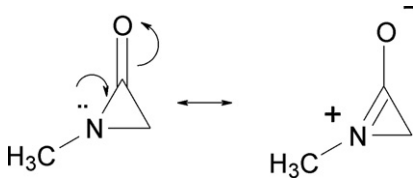

Scheme 4. Canonical forms which illustrate electron delocalization in the stable eliminated 1-methyl-aziridin-2-one, a 3-membered neutral cyclic product formed after fragmentation of $[M-H]^-$ ion.

C_3H_5NO elimination forms a cyclic 3-membered aromatic neutral and also decreases the aromaticity of the benzene ring in the formed phenylamide anion. Nucleus Independent Chemical Shift (NICS) was previously used to assess the aromatic/antiaromatic character of different organic neutral and ionic rings. The NICS value is defined as the (sign-reversed) isotropic NMR shielding contribution in the center of the ring. A negative NICS value indicates electronic ring current and aromaticity. NICS chemical shifts in the center of the amidic benzene ring gives a value of −6.1 ppm which is greater (less aromatic) than that of pure Benzene (−9.7 ppm) and of 1,2-dichlorobenzene (−11.2 ppm). The eliminated cyclic neutral product is aromatic with 2π electrons and NICS value of −26.8 ppm. The advantage of the NICS approach is its independency of ring size (unlike other methods for aromaticity determination such as diamagnetic susceptibility exaltation).

Fig. 10 shows Natural Bond Population (NBO) analysis for the charge distribution in the identified transition state which is responsible for this concerted elimination. The driving force for the cyclization of the eliminated neutral C_3H_5NO is the compensation of the charges in the formed ion-pair between N12 (−0.9 C) and C14 (+0.9 C). C17 with partial charge of −0.6 C can still act as a nucleophile and can add to the electrophilic carbon center C14 of the isocyanate moiety, to give a stable aromatic 3-membered ring with electron delocalization between the nitrogen atom and the external oxygen atom (Scheme 4). This electron delocalization further stabilizes the formed 3-membered cyclic ring.

7. Conclusion

Internal energy deposition on a formed ion can lead to intramolecular gas phase rearrangements prior to fragmentation. Multi acceleration events of ions can be achieved in a linear quadrupole, so that successive energy depositions can occur. However, not all energy depositions in the multi-step process lead to neutral eliminations. In some steps, proton shifts such that observed for dimethylamine loss from $[M-H]^-$ can take place to isomerize the anion and prepare it for fragmentation. Two

different main fragmentation pathways were discerned from the CID experiment of $[M-H]^-$ of DCMU. In case of C_3H_5NO elimination, a concerted mechanism was found which is in agreement with the NBO charge distribution of the associated transition state and NICS value for the stable aromatic ring. Thus, the driving force of this fragmentation is the formation of a stable 3-membered cyclic ring, which is not only stable due to its high aromaticity but also due to the electron delocalization with the external carbonyl group. The DFT approach reveals detailed information about the most probable mechanisms behind the observed gas phase fragmentation pathways of interesting organic ionic systems.

Acknowledgements

We thank Dr. Istvan Gebefügi for all his efforts in providing the facilities necessary to do this work.

Appendix A. Supplementary data

Supplementary data associated with this article can be found, in the online version, at doi:10.1016/j.ijms.2009.07.010.

References

[1] Environment Canada/Agriculture Canada, Pesticide Registrant Survey, 1987 report. Commercial Chemicals Branch, Conservation and Protection, Environment Canada, Ottawa, 1987.
[2] S.R. Sørensen, G.D. Bending, C.S. Jacobsen, A. Walker, J. Aamand, FEMS Microbiol. Ecol. 45 (2003) 1–11.
[3] B.T. Croll, B. Chadwick, B. Knight, Water Supply 10 (1992) 111–120.
[4] A. Trebst, W. Draber, Photosynth. Res. 10 (1986) 381–392.
[5] W. Oettmeier, Herbicides and photosystem, in: J. Barber (Ed.), Topics in Photosynthesis, Elsevier, Amsterdam, 1992, pp. 349–408.
[6] L.A. Kleczkowski, Annu. Rev. Plant Mol. Biol. 45 (1994) 339.
[7] E. Esposito, S.M. Paulillo, G.P. Manfio, Chemosphere 37 (1998) 541–548.
[8] C. Tixier, P. Bogaerts, M. Sancelme, F. Bonnemoy, L. Twagilimana, A. Cuer, J. Bohatier, H. Vaschambre, Pestic. Manag. Sci. 56 (2000) 455–462.
[9] A.K. Amina, B. Abdelaziz, P. Boule, Photochem. Photobiol. Sci. 3 (2004) 145.
[10] J.B. Foresman, A. Frisch, Exploring Chemistry with Electronic Structure Methods, Gaussian Inc., Pittsburgh, PA, USA, 1996, p. 64.
[11] B. Kanawati, F. Herrmann, S. Joniec, R. Winterhalter, G.K. Moortgat, Rapid Commun. Mass Spectrom. 22 (2008) 165.
[12] B. Kanawati, K.P. Wanczek, Int. J. Mass Spectrom. 264 (2007) 164–174.
[13] R.S. Kumar, A. Marwaha, P.V. Bharatam, M.P. Mahajan, J. Mol. Struct. 640 (2003) 1–12.
[14] A.K. Chandra, T. Uchimaru, J. Phys. Chem. A 104 (2000) 9244.
[15] A.K. Chandra, D. Michalska, R. Wysokinsky, T. Zeegers-Huyskens, J. Phys. Chem. A 108 (2004) 9593.
[16] A.D. Becke, J. Chem. Phys. 98 (1993) 5648–5652.
[17] P.J. Stephens, F.J. Devlin, C.F. Chabalowski, M.J. Frisch, J. Phys. Chem. 98 (1994) 11623–11627.
[18] H.F. Grützmacher, M. Büchner, H. Zipse, Int. J. Mass Spectrom. 241 (2004) 31.
[19] M. Büchner, H.F. Grützmacher, Int. J. Mass Spectrom. 228 (2003) 167.
[20] S. Naumov, I. Janovsky, W. Knolle, R. Mehnert, Phys. Chem. Chem. Phys. 6 (2004) 3933.
[21] D. Mariano, A. Vera, A.B. Pierini, Phys. Chem. Chem. Phys. 6 (2004) 2899.
[22] L. Ruiz-Gil, R. Romero-Gonzalez, A.G. Frenich, J.L.M. Vidal, J. Chromatogr. A 1150 (2007) 267–278.
[23] Garcia-Reyes, C. Ferrer, E.M. Thurman, A.R. Fernandez-Alba, I. Ferrer, J. Agric. Food Chem. 54 (2006) 6493.
[24] C.H. DePuy, J.J. Grabowski, V.M. Bierbaum, Science 218 (1982) 955.
[25] S. Kato, K.E. Carrigan, C.H. DePuy, V.M. Bierbaum, Eur. J. Mass Spectrom. 10 (2004) 225–231.
[26] J.H. Bowie, Mass Spectrom. Rev. 3 (1984) 161–207.
[27] H. Budzikiewicz, Mass Spectrom. Rev. 5 (1986) 345–380.
[28] B. Kanawati, S. Joniec, R. Winterhalter, G.K. Moortgat, Int. J. Mass Spectrom. 266 (2007) 97–113.
[29] B. Kanawati, S. Joniec, R. Winterhalter, G.K. Moortgat, Rapid Commun. Mass Spectrom. 22 (2008) 2269–2279.
[30] Y.H. Song, H. Chen, R.G. Cooks, Rapid Commun. Mass Spectrom. 19 (2005) 3493.
[31] J.A.A. Demmers, D.T.S. Rijkers, J. Haverkamp, J.A. Killian, A.J.R. Heck, J. Am. Chem. Soc. 124 (2002) 11191.
[32] H. Lioe, R.A.J. O'Hair, G.E. Reid, J. Am. Soc. Mass Spectrom. 15 (2004) 65.
[33] T.J.D. Jorgensen, H. Gardsvoll, M. Ploug, P. Roepstorff, J. Am. Chem. Soc. 127 (2005) 2785.
[34] P. Caravatti, M. Allemann, Org. Mass Spectrom. 26 (1991) 514.
[35] B. Kanawati, K.P. Wanczek, Rev. Sci. Instrum. 78 (2007) 074102.
[36] B. Kanawati, K.P. Wanczek, Int. Mass Spectrom. 269 (2008) 12–23.
[37] B. Kanawati, K.P. Wanczek, Int. Mass Spectrom. 274 (2008) 30–47.
[38] M.J. Frisch, G.W. Trucks, H.B. Schlegel, G.E. Scuseria, M.A. Robb, J.R. Cheeseman, J.A. Montgomery Jr., T. Vreven, K.N. Kudin, J.C. Burant, J.M. Millam, S.S. Iyengar, J. Tomasi, V. Barone, B. Mennucci, M. Cossi, G. Scalmani, N. Rega, G.A. Petersson, H. Nakatsuji, M. Hada, M. Ehara, K. Toyota, R. Fukuda, J. Hasegawa, M. Ishida, T. Nakajima, Y. Honda, O. Kitao, H. Nakai, M. Klene, X. Li, J.E. Knox, H.P. Hratchian, J.B. Cross, V. Bakken, C. Adamo, J. Jaramillo, R. Gomperts, R.E. Stratmann, O. Yazyev, A.J. Austin, R. Cammi, C. Pomelli, J.W. Ochterski, P.Y. Ayala, K. Morokuma, G.A. Voth, P. Salvador, J.J. Dannenberg, V.G. Zakrzewski, S. Dapprich, A.D. Daniels, M.C. Strain, O. Farkas, D.K. Malick, A.D. Rabuck, K. Raghavachari, J.B. Foresman, J.V. Ortiz, Q. Cui, A.G. Baboul, S. Clifford, J. Cioslowski, B.B. Stefanov, G. Liu, A. Liashenko, P. Piskorz, I. Komaromi, R.L. Martin, D.J. Fox, T. Keith, M.A. Al-Laham, C.Y. Peng, A. Nanayakkara, M. Challacombe, P.M.W. Gill, B. Johnson, W. Chen, M.W. Wong, C. Gonzalez, J.A. Pople, Gaussian 03, Revision D, Gussian, Inc., Wallingford, CT, 2004.
[39] H.B. Schlegel, J. Comput. Chem. 3 (1982) 214–218.
[40] P. Csaszar, P. Pulay, J. Mol. Struct. 114 (1984) 31–34.
[41] O. Farkas, H.B. Schlegel, Phys. Chem. Chem. Phys. 4 (2002) 11–15.
[42] O. Farkas, H.B. Schlegel, J. Chem. Phys. 111 (1999) 10806.
[43] C. Gonzalez, H.B. Schlegel, J. Chem. Phys. 90 (1989) 2154–2161.
[44] C. Gonzalez, H.B. Schlegel, J. Phys. Chem. 94 (1990) 5523–5527.
[45] P.V. Schleyer, C. Maerker, A. Dransfeld, H.J. Jiao, N. Hommes, J. Am. Chem. Soc. 118 (1996) 6317–6318.
[46] J.L. Dodds, R. McWeeny, A.J. Sadlej, Mol. Phys. 41 (1980) 1419.
[47] K. Wolinski, J.F. Hilton, P. Pulay, J. Am. Chem. Soc. 112 (1990) 8251.
[48] Roy Dennington II, Todd Keith, John Millam, Ken Eppinnett, W. Lee Hovell, Ray Gilliland, GaussView, Version 3.0.9, Semichem Inc., Shawnee Mission, KS, 2003.
[49] P.V. Bharatam, R. Moudgil, D. Kaur, J. Phys. Chem. A 107 (2003) 1627–1634.
[50] M. Diefenbach, H. Schwarz, Chem. Eur. J. 11 (2005) 3058–3063.
[51] G.S. Hammond, J. Am. Chem. Soc. 77 (1955) 334–338.